Hydrol. Earth Syst. Sci. Discuss., 9, 7699–7738, 2012
www.hydrol-earth-syst-sci-discuss.net/9/7699/2012/
doi:10.5194/hessd-9-7699-2012

Hydrology and Earth System Sciences Discussions

Origin and assessment of deep groundwater inflow in the Ca' Lita landslide using hydrochemistry and in situ monitoring

F. Cervi[1], F. Ronchetti[1], G. Martinelli[3], T. A. Bogaard[2], and A. Corsini[1]

[1]Department of Earth Sciences, University of Modena and Reggio Emilia, Italy
[2]Department of Water Management, Delft University of Technology, The Netherlands
[3]Regional Agency for the Protection of the Environment (ARPA), Emilia Romagna, Italy

Received: 9 May 2012 – Accepted: 26 May 2012 – Published: 14 June 2012

Correspondence to: F. Cervi (federico.cervi@unimore.it)

Published by Copernicus Publications on behalf of the European Geosciences Union.

Abstract

Changes in soil water content, groundwater flow and a rise in pore water pressure are well-known causal or triggering factors for hillslope instability. Rainfall and snowmelt are generally assumed as the only sources of groundwater recharge. This assumption neglects the role of deep water inflow in highly tectonized areas, a factor that can influence long-term pore-pressure regimes and play a role on local slope instability.

This paper aims to assess the origin of groundwater in the Ca' Lita landslide (northern Italian Apennines) and to qualify and quantify the aliquot attributable to deep water inflow. The research is essentially based on in situ monitoring and hydrochemical analyses. It involved 5 yr of continuous monitoring of groundwater levels, electrical conductivity and temperature, and with groundwater sampling followed by determination of major ions, tracers (such as Boron and Strontium), and isotopes (Oxygen, Deuterium, Tritium). Leaching experiments on soil samples and water recharge estimation were also carried out.

Results show that the groundwater balance in the Ca' Lita landslide must take into account an inflow of highly mineralized Na-SO_4 water (more than 9500 $\mu S\,cm^{-1}$) with non-negligible amounts of Chloride (up to 800 $mg\,l^{-1}$). The deep water inflow recharges the aquifer hosted in the bedrock underlying the sliding surface (at a rate of about 7800–17 500 $m^3\,yr^{-1}$). It also partly recharges the landslide body, where the hydrochemical imprint of deep water mixed with rainfall and snowmelt water was observed. This points to a probable influence of deep water inflow on the mobility of the Ca' Lita landslide, a finding that could be applicable to other large landslides occurring in highly tectonized areas in the northern Apennines or in other mountain chains.

1 Introduction

Instability of hillslopes is generally triggered by hydrological and hydrogeological factors governing infiltration, increase of pore water pressure, and resulting decreases in

HESSD

9, 7699–7738, 2012

effective stress in the soil (Wieczorek, 1996; van Asch et al., 1999). In deep-seated landslides, effective groundwater infiltration on a slope scale over long periods of time can increase hydrostatic levels and determine groundwater flow, thus playing an important role in the reactivation of slope movements (Hutchinson, 1970; Iverson and Major, 1987; van Asch et al., 1999).

However, the activation/reactivation of deep-seated landslides is a complex issue and groundwater recharge is not always due to precipitation alone. For instance, deep water upflow along regional tectonic structures can affect groundwater balance on a slope scale (Tóth, 1999). The presence of deep water into landslide deposits was reported in several cases in the northern Apennines (Baraldi, 2008; Bertolini and Gorgoni, 2001; Ciancabilla et al., 2004; Colombetti and Nicolodi, 1998; Ronchetti et al., 2009) as well as in other mountain chains (Bonzanigo et al., 2001; de Montety et al., 2007).

Deep water can easily be detected by hydrochemical surveying (Bogaard et al., 2007) due to its very distinct chemical imprint depending on depth, temperature, and pressure conditions, the mineral composition of hosting rocks or deposits, time of interaction between water and aquifer, and the mixing of different water types (Freeze and Cherry, 1979). However, differentiation of water types in hillslope hydrology is not often conducted (Guglielmi et al., 2000; Cappa et al., 2004).

This paper deals with the analysis of groundwater in the Ca' Lita landslide, a large rotational rock slide-earth flow affecting highly tectonized flysch rock masses in the northern Italian Apennines. The landslide occurs along a major regional fault line, through which deep water inflow is believed to occur. The aim is to assess the origin of groundwater below and inside the landslide, and to qualify and quantify the aliquot of groundwater from deep water inflow. The research makes combined use of groundwater monitoring and chemical/isotopic analyses. The results allow an assessment of the contribution of deep water to the hydrological processes and development of instability involved in the landslide.

HESSD
9, 7699–7738, 2012

2 Hydrogeological and hydrochemical context of the northern Apennines

The northern Apennines (NA) are a fold-and-thrust mountain belt generated by the closure of the Ligure-Piemontese Ocean basin and the subsequent collision of the Adria and European continental plates (Boccaletti et al., 1971; Klingfield, 1979; Bettelli and Vannucchi, 2003; Molli, 2008). As a consequence of the polyphasic evolution of the accretionary wedge, the northern Apennines are made up of several tectono-stratigraphic units of marine sedimentary rocks (Fig. 1). The Tuscan Unit (TU), the Ligurian Unit (LU), and the Sestola Vidiciatico Unit (SV) are mainly composed of thick and highly tectonized turbidite sequences (flysch rock masses) and clayey chaotic deposits (clayshales). Within these units, Triassic evaporites (TUG gypsum) are also found. The Epiligurian Unit (EL) is mainly composed of turbidites (flysch rock masses). The Messinian and Post Messinian units, outcropping only at the front of the mountain chain, are made up of evaporites (MME gypsum) and marine clayey rocks (QM). The main hydrogeological characteristics of these units and the typical hydrochemical imprint of hosted groundwater are described below.

2.1 Tuscan Units (TU)

Groundwater circuits developing within TU flysch rock masses are mostly shallow and widely distributed. The unconfined aquifers feed a large number of low-yield springs which discharge where the groundwater table crosses the land surface or a permeability contrast occurs. A deep regional groundwater flow system (Base Regional System – BRS sensu Tóth, 1999) has recently been identified by Gargini et al. (2008): it slowly (from 10^{-12} to 10^{-14} m s^{-1}) moves from the upper NA chain toward the Po Plain. Supplied by rainfall and snowmelt water infiltrating near the watershed divide, the BRS is driven by regional gradients, but in some cases tectonic lineaments or topography concentrate discharge in isolated springs or directly into stream beds.

Systematic changes in the anion facies have been reported: fresh infiltrated waters start from HCO_3 (point no. 5 in Fig. 1a, b) and pass through SO_4 (point no. 7)

HESSD
9, 7699–7738, 2012

finally reaching Cl (point no. 4), while TDS (Total Dissolved Solids) increases up to 9–10 $g\,l^{-1}$. pCO_2 constantly increases up to 2.0 kPa. Water stable isotopes (O^{18} and ^2H) range within precipitation values, shifted towards negative values, which characterize the higher recharge areas ($\delta^{18}O$ up to −10.5 to −11 while δ^2H can reach −75: Gargini et al., 2008).

In the longer and deeper flow paths (main anion: Cl), accumulation of trace ions, such as B and Sr and transported hydrocarbons and/or immiscible fluids (oil, gas) were noted (point no. 4 in Fig. 1a, b: Minissale et al., 2000; Capozzi and Picotti, 2002; Heinicke et al., 2010). In several cases their content is strongly related; B, which can be mobilized from the organic matter buried during sedimentary processes, is normally associated with oilfield water if its value is in the order of 100 $mg\,l^{-1}$ (White, 1965) while Sr ranges from 100 to 500 $mg\,l^{-1}$ (Conti et al., 2000; Capozzi and Picotti, 2010).

2.2 Sestola-Vidiciatico Unit, Ligurian Units and Epiligurian Units (SV, LU and EL)

Moving towards the middle-front portion of the wedge, the SV and LU units can be considered impermeable. Starting from the 1950s, the LU has been subjected to several drilling campaigns for intensive hydrocarbon investigations (results are collected inside the national VIDEPI Project: http://unmig.sviluppoeconomico.gov.it/videpi/en/). Many oil wells (Viano, Baiso, Serramazzoni in Fig. 1a) passing through the clayey formations found impregnation (even salience) of salt water (Na-Cl up to 9 $g\,l^{-1}$) together with oil and gas emission (methane, superior hydrocarbon, nitrogen). Like these, other spontaneous emissions (point no. 3c in Fig. 1a) flowing out from the same unit show similar chemical characteristics (salinity up to 11 $g\,l^{-1}$). Their water isotopes are positive ($\delta^{18}O$ around $+5 \div +6$) while pCO_2 stays around 1 kPa (Conti et al., 2000; Capozzi and Picotti, 2010).

EL flysch acts as an aquifer and stores Ca-HCO_3 water (point no. 5 in Fig. 1a, b). During the warm season springs provide discharge in the order of few $l\,s^{-1}$ and low ion content (salinity is normally lower than $0.8 \div 1\,g\,l^{-1}$ with pCO_2 ranging from 0.6 to

HESSD
9, 7699–7738, 2012

1.9 kPa). The isotopic imprint corresponds to the local recharge area ($\delta^{18}O$ between −8.5 and −11, $\delta^{2}H$ between −55 and −75) (Minissale et al., 2000; Cremaschi, 2009). Sr is normally lower than 1 mg l^{-1} while B doesn't exceed 0.05 mg l^{-1} (Duchi et al., 2005; Toscani et al., 2001).

2.3 Triassic (TUG) and Messinian (MME) evaporites

In gypsum formations belonging to the TUG and MME, fresh water springs (point no. 6 in Fig. 1a, b) can originate. This water has high SO_4 values and, if the aquifer consists of halite, also Cl. Salinity is normally higher than 2–3 g l^{-1} while Sr and B contents are lower than 15 mg l^{-1} and 2 mg l^{-1}, respectively (Chiesi et al., 2010; Duchi et al., 2005; Toscani et al., 2001). pCO_2 is between 0.03–0.3 kPa. Isotope composition reflects the recharge altitude ($\delta^{18}O$ between −8.5 and −11, $\delta^{2}H$ between −55 and −75: Cervi, 2003).

2.4 Post Messinian Units (QM)

Along the boundary with the Po plain, several mud volcanoes (points 3a, b in Fig. 1a, b) affect the impermeable QM. These phenomena, which are widely observed along compressive margins around the world (Martinelli and Judd, 2004; Martinelli and Dadomo, 2005), consist of Na-Cl waters (up to 90 g l^{-1}) flushing out particles of clay and entrapped connate water of the old pliocenic sea (Bonini, 2007). They originate from the buried QM-TU contact (located at a depth of more than 2000 m) whereas oilfield fluids start to rise up towards the surface following inverse faults. Stable isotopes (^{18}O and ^{2}H) are sometimes highly positive ($\delta^{18}O$ up to +5 and $\delta^{2}H$ equal to 0) while pCO_2 varies widely (0.03–0.9 kPa). B and Sr can be as high as 300 mg l^{-1} (Boschetti et al., 2010).

HESSD
9, 7699–7738, 2012

3 Ca' Lita landslide context

The Ca' Lita landslide is located between 640 and 230 m a.s.l. in the NE slope of the northern Apennines. Over the last 40 yr, the average annual rainfall in the area was 810 mm yr^{-1} and the mean air temperature was 11.7 °C (http://www.arpa.emr.it). Precipitation is distributed over 70 to 100 days yr^{-1} with two peaks: a main one in autumn (October–November) and a secondary one in spring (April). Fazlagic et al. (2004) report an average annual snowfall of about 42 cm from 1830 to 1998.

The Ca' Lita landslide affects a hillslope composed of formations belonging to the Ligurian Units (LU). One formation consists of poorly cemented sandstone flysch (MOH), another is composed of clayshales (MVR) (Fig. 2a, b). In the slope, the stratigraphic relation between MOH and MVR is complicated by the presence of a high angle regional fault (Papani et al., 2002).

The landslide can be classified as a reactivated complex landslide (WP/WLI, 1993; Cruden and Varnes, 1996), associating rotational rock slides in the crown and head zones (in the MOH formation) with earth flows in the lower main body (in the MVR formation). It was reactivated several times in the last century (Borgatti et al., 2006; Corsini et al., 2009). Recently, it resumed activity in 2002 and underwent paroxysmal phases in winter 2003 and spring 2004 due to 200 mm of cumulated rainfall in the two preceding months combined with the rapid melting of about 80 cm of snow.

After the 2004 event, an extensive geological investigation and monitoring campaign was set up in order to design mitigation structures (Corsini et al., 2009). Boreholes and inclinometers showed that the active rock slide deposit had a maximum thickness of 44–48 m while the active earth flow deposit had a mean thickness of about 10 m (Borgatti et al., 2006). Since summer 2006, no further deep seated rock slide movements have been recorded and only shallow slides have occurred close to the main scarps.

Later, inclinometers and 5 standpipe piezometers were installed and equipped with pressure transducers. Electrical conductivity probes were also fitted inside two of these. Piezometers were used in the research as groundwater monitoring and sampling

HESSD
9, 7699–7738, 2012

points. Other monitoring and sampling points were drainage wells and sub-horizontal drains constructed during mitigation work at different locations in the slope (Fig. 2a, b). Deep drainage wells in the rock slide drain groundwater from the landslide body and convey it to well A (WA in Fig. 2a, b), from where it is removed by pumping. At the base of the frontal scarp of the rock slide zone, a shield of shallow drainage wells drain water from the superficial debris and convey it to drainage point B (DrB in Fig. 2a, b). In the same area, a set of sub-horizontal drains of length from 50–100 m drain water from the bedrock below the sliding surface and convey it to drainage point A (DrA in Fig. 2a, b).

4 Methods

With reference to the case study, an interdisciplinary investigation was performed. It consisted of several steps involving hydrological (groundwater level and discharge monitoring, estimation of the groundwater balance for several hydrologic years), hydrochemical (groundwater conductivity monitoring, groundwater isotopic and chemical analyses, leaching experiments, hydrochemical modelling), and mineralogical (soil composition) surveys.

More specifically, the groundwater chemistry and stable isotope contents were characterized in order to assess end-members and mixing phenomena. An independent validation, to check if the peculiar water chemistry could be due only to the mineralogy of the site, consisted in leaching experiments with soil samples belonging to the two outcropping geological formations. In addition, another equilibrium-based model PHREEQC (Parkhurst and Appelo, 2004) was defined in order to simulate the long-term chemical interaction between rainfall water and host rocks.

The aliquot of deep water was estimated by coupling radioactive isotopes content with groundwater balance.

HESSD
9, 7699–7738, 2012

4.1 Groundwater level, conductivity and discharge monitoring

The 5 standpipe piezometers are slotted at different depths and monitor groundwater in the bedrock at the crown and along the side of the rock slide (P1, P2), inside the rock slide body (P3), and across the deepest sliding surface (P4, P5) (Fig. 2a, b). The characteristics of the boreholes are reported in Table 1.

They have been equipped with pressure transducers since 2005 in order to monitor groundwater levels (GW_L) with an acquisition frequency of 1 h. Electrical Conductivity (GW_{EC}) was measured from June 2009 to March 2010, with an acquisition frequency of 6 h in P3 and P4. In the other piezometers, GW_{EC} and groundwater temperatures (GW_T) were measured periodically from 2006 to 2009 and from 2010 to date.

The discharge of groundwater drained by the wells from inside the rock slide body was monitored from 2007 to 2010 by means of a graduated weir located at the outlet of the WA pumping system. The discharge of groundwater drained by sub-horizontal drains from the bedrock underneath the main rock sliding surface was monitored from 2006 to 2009 by means of a graduated weir located at the outlet of DrA. In WA and DrA, the GW_{EC} and the GW_T were measured seasonally from 2006 to August 2010. The physical-chemical parameters were checked using a Crison MM40+ multimeter equipped with a Ross glass electrode for pH.

4.2 Groundwater chemical analyses

Groundwater sampling was conducted in 2006 (sampling campaign A), 2007 and 2009 (sampling campaigns B and D; red square in Fig. 3b). All the 5 standpipe piezometers and both DrA and DrB were sampled. All samples were collected using bailers except samples collected during summer 2009 from DrA and P1, which were collected using a low-flow pump (0.1 l s^{-1}) after removing the standing water in the piezometer. Water for laboratory study was filtered through 0.45-µm cellulose membranes, and the aliquot for cation analysis was acidified with 65 % HNO_3 Suprapur Merck.

HESSD
9, 7699–7738, 2012

Analyses were conducted to establish major ion concentrations (K, Na, Cl, Ca, Mg, SO_4 and HCO_3) as well as the B and Sr contents. Cation contents were assessed by atomic absorption spectrometry (Spectr AA-640, Varian). Anions were determined using an HPLC (high performance liquid chromatography, Dionex DX-120). Total alkalinity was assessed by Gran titration (Gran, 1952). Data are reported in $mg\,l^{-1}$ (Table 3).

4.3 Groundwater isotopic analyses

Stable oxygen and hydrogen isotope analyses (^{18}O, ^{2}H) were carried out by mass spectrometry on water samples collected from all the piezometers and DrA.

Five sampling campaigns scattered over 3 yr were conducted starting from 2007 (sampling campaigns B, C, D, E, F; yellow diamond in Fig. 3b). The samples represent the summer (B, D, F), winter (C), and spring (E) periods. The results are reported as differences between the sample and the standard (Vienna Standard Mean Oceanic Water: V-SMOW). This deviation is presented in the standard δ-notation as per mil (‰) where $\delta = [(R_S/R_{SMOW}) - 1] \cdot 1000$; R_S represents either the $^{18}O/^{16}O$ or the $^{2}H/^{1}H$ ratio of the sample, and R_{SMOW} is $^{18}O/^{16}O$ or the $^{2}H/^{1}H$ ratio of the SMOW.

In August 2010 (sampling campaign F; green diamond in Fig. 3b), Tritium analysis (^{3}H) was carried out on water collected from DrA in order to determine Tritium Units (T.U. in which one T.U. equals one tritium atom per 10^{18} hydrogen atoms). Analysis was performed using the electrolytic enrichment and liquid scintillation counting method (Thatcher et al., 1977). Due to the chemical content, DrA was selected as representative of the deepest and longest circulation path developed through the landslide area while stream water flowing a few km north of Ca' Lita (Secchia river; Regione Emilia-Romagna-ARPA, 2009) was used as a "benchmark" representing the mean ^{3}H value for local rainfall.

HESSD
9, 7699–7738, 2012

4.4 Leaching analyses

Four soil samples from the two different geological formations (MVR and MOH) were collected from in-situ outcrops (about 7 km south of Ca' Lita, Fig. 1a: MVRb and MOHb) and regolith (i.e. weathered material still in its original location at Ca' Lita, Fig. 1a: MVRa and MOHa). According to the USGS Field Leach Test (2005), 50 g of dried material for each sample was sieved less than 2 mm and leached into 1 l of deionised water, continuously shaken by a magnetic agitator (with a constant rotation speed of 200 rpm). The experiments extended over a maximum of 10 h while an electrical conductivity probe was used to monitor water mineralization on a fixed time-table (30 s, 1 m, 2 m, 5 m, 10 m, 30 m, 1 h, 10 h). Each water sample was collected after 1 h of interaction to determine the major ion contents.

4.5 Mineralogical analyses and PHREEQC modelling

The mineralogy was investigated using 2 soil samples collected at Ca' Lita (MOHa, MVRa). The analysis of the <2 µm fraction was conducted using X-ray diffractometry on oriented paste. Starting from these two mineralogical assemblages, the PHREEQC model simulates the interaction (precipitation and dissolution of phases) with an aqueous solution (specifically: rain water with a mean temperature equal to the mean annual air temperature of the site, i.e. 11.7 °C and pH = 5.8) until equilibrium is reached.

4.6 Groundwater balance

The mean annual groundwater recharge from rainfall was estimated using rainfall and temperature data over the last 40 yr derived from available official databases (http://www.arpa.emr.it) for the nearest weather station (Baiso), located 4.5 km northwest of Ca' Lita with the same elevation and aspect. The Thornthwaite and Mather (1957) formula was used to assess the potential mean annual evapotranspiration. Total groundwater recharge volume was calculated by multiplying the water surplus for the slope

HESSD
9, 7699–7738, 2012

recharge area. The mean annual groundwater recharge from deep water inflow was estimated by solving a simplified annual water-balance equation and processing the ^{3}H data as described by Mazor (1997).

5 Results

5.1 Groundwater monitoring

The main groundwater recharge into the slope takes place in the autumn and spring when the effective rainfall is available. Similarly to the rainfall pattern, the GW_L, has two peaks (Table 2) one in November/December and another in April. These are normally followed by groundwater regression periods; the main one between May and October. GW_L patterns are reported in Fig. 3a. In the crown area (P1), the groundwater response delay after rainfall events is in the order of a few hours up to a couple of days, while the GW_L can increase by more than 5 m. These GW_L peaks then discharge completely within 5–10 days. The maximum seasonal amplitude is about 7 m. The flysch rock mass in the crown is intensively fractured (P2) and behaves differently. GW_L variations for each event are modulated or even absent (as the consequence of high hydraulic conductivity). However, during an intensive rainfall-recharge period, an increase of more than 10 m was detected. In the head zone, above the main sliding surface (P3), GW_L are affected by the high-frequency pumping in WA; as a result, they are stabilized at about 29 m from the ground surface.

In the deepest piezometers, which monitor deep multi-compartmented horizons (P4, P5: since the records are overlapping, only the second is represented in Fig. 3a), GW_L are about 20 m higher than the GW_L observed inside the main landslide body (P3). Only the most intense precipitations (such as 150 mm on 10 June 2008) can influence the GW_L record (total head increased by 1 m after 1 month) while seasonal peaks are modulated (2–4 m) and shifted by some months compared to the rainfall records.

HESSD
9, 7699–7738, 2012

Despite GW_{EC} continuous monitoring only being available for the head zone, different trends can be observed (Fig. 4). Above the sliding surface (P3), a continuous decrease in GW_{EC} is evident. Starting from 5450 $\mu S\,cm^{-1}$, it fell to a final value of around 5100 $\mu S\,cm^{-1}$ with a minimum of 4570 $\mu S\,cm^{-1}$ on 22 October 2009. This drop was the result of automatic pumping switching-on in WA and the consequent downflow of less mineralized water coming from the shallow part of the landslide body. A new equilibrium was reached only after 3 months (5100 $\mu S\,cm^{-1}$). In summer 2011, due to continuous pumping, GW_{EC} reached a new minimum value of 1247 $\mu S\,cm^{-1}$. For the same time window, GW_{EC} measured in P4 increased from 5500 to 5800 $\mu S\,cm^{-1}$ with a smoothed peak of more than 6000 $\mu S\,cm^{-1}$ in November 2010. The latter was preceded by 300 mm of effective rainfall over 3 months, which provided slight GW_L increases even in the deepest piezometers (P2).

The discharge monitoring network started to collect data in 2006–2007 and was stopped in 2009 (WA) and so only the hydrologic year 2007–2008 is available for further comparison, when a total of 30 000 m^3 was drained from WA and 6000 m^3 from DrA.

5.2 Groundwater chemical analyses

Groundwater salinity ranged between a minimum value of about 1.5 $g\,l^{-1}$ measured in the upper part of the slope (P1), to 6 $g\,l^{-1}$ measured in the lower part of the slope (DrA, sampling campaign F). According to Drever (1977), the latter can be classified as salt (brackish) water. These waters are enriched in Na and SO_4 with substantial amounts of HCO_3 (up to 1100 $mg\,l^{-1}$) and a significant content of chlorides (up to 787 $mg\,l^{-1}$ in DrA). pCO_2 ranged from about 6 kPa (P4) to 1.4 kPa (DrA), while pH fluctuated around 7 (slightly acid in the upper part of the slope: 6.6–6.9 observed in P1).

The most mineralized water collected at Ca' Lita during sampling campaign A (DrA) is reported in a Piper diagram together with other GW of NA (Fig. 5a). Whereas common shallow GW falls on the left side of the diamond, the Ca' Lita sample plots in the

HESSD
9, 7699–7738, 2012

right corner (Na-SO_4 GW-type). This hydrofacies characterizes all water sampled at Ca' Lita (Fig. 5b), with P4 shifted downwards owing to the higher HCO_3 content.

Regarding the main ion contents (reported in Table 3), P3, P5 and DrB had the lower values for both ions (Na of about 500–600 $mg\,l^{-1}$ and SO_4 800–1000 $mg\,l^{-1}$) while the other samples exceeded 800 $mg\,l^{-1}$ and 1000 $mg\,l^{-1}$, respectively.

Marked discrepancies were detected in the Chloride contents. The head zone (P3, P4, P5) is characterized by lower levels of Cl (less than 90 $mg\,l^{-1}$). The piezometers inserted inside the flysch rock masses (P1, P2) reached 300–400 $mg\,l^{-1}$ with a maximum of 790 $mg\,l^{-1}$ in DrA.

A comparison between sampling campaigns A, B and D was only possible for P1 and DrA. In 2009 (sampling campaign D) the Cl contents were halved, while Na and SO_4 slightly increased. The most pronounced increase involved DrA: in this case, Na increased to about 1600 $mg\,l^{-1}$ while SO_4 tripled (more than 3000 $mg\,l^{-1}$). This fact is responsible of the upward displacement of the last DrA sample in the Piper diagram (Fig. 5b).

Trace ion levels are available only for the last sampling campaign: B concentrations reached 8.2 $mg\,l^{-1}$ (DrA) and 6.4 $mg\,l^{-1}$ (P1); Sr varied from 6.8 (DrA) to 3.3 (P1) $mg\,l^{-1}$.

5.3 Groundwater isotopic analyses

The isotopic values $\delta^{18}O$ and $\delta^{2}H$ are reported in Table 3. Several samples from the landslide body (P4, P5) or the lateral unstable crown (P2) were characterized by depleted values of $\delta^{18}O$ which ranged from −8.5 to −9.5. In one case (P5), $\delta^{18}O$ did not change over the seasons (−9.13; −9.23). These mean values are more negative than the isotopic signal which characterized the mean annual rainfall for this altitude ($\delta^{18}O$ ranging from −7.8 to −8 for an elevation between 600 and 650 m a.s.l.; Longinelli and Selmo, 2003). That is consistent with the water-balances calculated for the same time-window (see Sect. 7). In fact, it can be expected that recharging is concentrated in the

HESSD
9, 7699–7738, 2012

late autumn to early spring when rainfall and snowmelt provide more depleted isotopic values (Iacumin et al., 2009).

In P1 and DrA, $\delta^{18}O$ values are even less depleted than those characterizing the meteorological observations (up to −6.51 and −5.33, respectively, in July 2007). As soon as the mitigation system began to drain GW in the head zone, $\delta^{18}O$ in P1 and DrA started to become more negative (the first reached −7.90 in June 2009 while the other reached −6.93 in summer 2010).

All the samples were plotted in a $\delta^{18}O$-$\delta^{2}H$ graph (Fig. 6). Several points (DrA, P1, P2) are clearly shifted downwards from the local meteoric line (northern Italy meteoric line by Longinelli and Selmo, 2003); this is due to a slight negativization of the ^{2}H isotope which becomes highly-depleted in DrA (from −49.23 to −53.54). The other piezometers lie on the local meteoric line.

The ^{3}H content in GW flowing out of DrA during summer 2010 was significantly lower than the mean isotopic value characterizing the rainfall in NA (3.5 and 10 T.U., respectively; the latter was obtained from a monthly dataset that includes the hydrologic year 2009).

5.4 Leaching analysis

Table 4 summarizes the results of the leaching experiments. The time required to reach the final concentration was generally short for all the samples: at least 70 % of the total chemical content was achieved within 10 min, and 90 % within 1 h. Clearly, the 1 h samples are representative of the lixiviation interactions between soil and water.

Once leached, all the MOHa and MOHb provided Ca-HCO_3 water with similar mineralization (close to 200 µS cm^{-1} after 1 h). Otherwise, appreciable differences were detected between MVR samples. In particular, an increase of mineralization (up to 930 µS cm^{-1} while the furthest sample MVRb remained around 180 µS cm^{-1}) was noticed in MVRa. Starting from the Ca-HCO_3 water of the former, the samples leached with MVRa soil collected along the main fault were enriched with Na and SO_4 up to

HESSD
9, 7699–7738, 2012

160 and 175 mg l^{-1}, respectively. These results are only partially in agreement with the chemical characteristics of the water hosted in the deepest aquifer of Ca' Lita (DrA). In this case, unlike the water collected from DrA, only few mg l^{-1} of Cl were detected during the leaching experiment.

5.5 PHREEQC modelling

The composition of the flysch rock mass (MOH) was established as 33.6 % clay (25 % smectites, 25 % chlorites, 41 % illites, 8 % kaolinite), 55.8 % quartz, 2 % calcite, and 8.6 % feldspar. MVR is mainly composed of clay (about 78 %: 89 % smectites, 8 % kaolinite, and some traces of illites) together with 7.8 % quartz, 13.3 % calcite and 1.2 % feldspar.

In the PHREEQC modeling two different scenarios were tested according to the state of the hydrogeological system: in the first, it was considered as closed to the surface (pCO_2 reached values of 2.5 kPa and 3 kPa, respectively), while in the second a fixed partial pressure of CO_2 was guaranteed (pCO_2 equal to 0.03 kPa). In both cases, some ions showed discrepancies even with the results obtained from the leaching experiment. Mg was not present in the final solution (<0.1 mg l^{-1}) while Ca was assessed as around 2–4 mg l^{-1}. Sodium content was increased through albite dissolution, reaching 100 mg l^{-1} (closed system) and some thousands in the second case. Regarding anion contents, only HCO_3 (more than 100 mg l^{-1}) could be produced by these assemblages of minerals while no SO_4 was detected.

6 Discussion: origin of groundwater and conceptual model of deep water inflow

Results suggest the existence of a complex hydrogeological system comprising overlapping aquifers characterized by the presence of Na-SO_4 GW.

In the landslide body (head zone), the aquifer hosted above the main sliding surface (P3) exhibits an unconfined behaviour (Fig. 2b). Its response to rainfall events

HESSD
9, 7699–7738, 2012

is brief. The same patterns can be noticed in GW_{EC}: values range between 1000 to 5000 $\mu S\,cm^{-1}$.

Below the sliding surface (P4 and P5), in the thick deformation band made up of disarranged flysch, the same aquifer becomes semi-confined (or multi-compartmented). GW_L have no direct relationships with rainfall as only modulated (changes less than 5 m) seasonal variations are observed. P4 had higher GW_{EC} values and ion contents, together with less depleted values of $\delta^{18}O$ (between −8.5 and −8.7 compared to −9.5 observed for P5).

However, in both cases the chemical imprints are quite similar and characterized by low Cl contents (less than 88 $mg\,l^{-1}$).

All the water samples taken lie on the local meteoric isotopic line, and the most depleted values of $\delta^{18}O$ (close to −9.5) can be assumed to be strongly linked to infiltration processes, representing natural rain gauges for the mean annual isotopic rainfall content.

The aquifer hosted in the undisturbed flysch (P1 and DrA) and in the side crown (P2) behaves differently. Depending on the denser and more persistent fracturing pattern characterizing the crown zone, GW_L variations in P1 are higher than those detected in P2. However, both piezometers are characterized by water depleted in $\delta^{2}H$ together with high contents of Cl (300–400 $mg\,l^{-1}$). The latter reaches about 800 $mg\,l^{-1}$ at the bottom of the aquifer (DrA). Discharged water is the most highly mineralized (GW_{EC} up to 9500 $\mu S\,cm^{-1}$).

A sharp decline in chemical parameters occurred during November 2009: EC in the landslide body repositioned at about 1500 $\mu S\,cm^{-1}$ (P3). Due to the continuous pumping in WA, the unconfined aquifer hosted in the head zone was progressively renewed by the inflow of more fresh and less mineralized water from the upper landslide body. This presence was confirmed by Ronchetti et al. (2009) after conductivity loggings in P1: the authors detected a rapid increase with depth of GW_{EC} (stabilized at about 4000 $\mu S\,cm^{-1}$ at 20 m below the water table). The other aquifers were also affected by

HESSD
9, 7699–7738, 2012

the hydrological changes in the head zone: in some cases (P1 and DrA) Cl levels were halved.

This change was also observed in the δ^{18} record. In DrA, δ^{18} decreased from −5.33 in July 2007 to −6.93 in August 2010. This can be interpreted as the result of an increased contribution of lighter rain water infiltrating into bedrock from the upper landslide body, thus producing a mixture of shallow and deep groundwater. A reference value for the mean annual δ^{18} for shallow groundwater can be obtained from P5, which is constantly close to $\delta^{18} = -9.13$. On the other hand, an indicative value for the mean annual δ^{18} of deep groundwater of +5.5 can be estimated by considering an aliquot of deep water inflow in the order of 500 000 m^3 (as described in further detail in Sect. 7, this value can be estimated on the basis of ^{3}H measured in DrA and of the reconstructed geometry and storativity of the MOH reservoir). An estimated value of δ^{18} of +5.5 for deep water inflow is also consistent with δ^{18} values measured in mud volcanoes located 15 km to the north (points no. 3a, b in Fig. 1a) as well as in other springs flowing out of TU flysch formations (i.e. Well Salsmag1 in Boschetti et al., 2010) or from LU-TU formations in the middle-frontal part of the Apennine chain (i.e. Regnano site, point 3c in Fig. 1a; Capozzi and Picotti, 2010).

Other evidence supports the hypothesis of mixing between deep water inflow and rainfall-recharge water inside the bedrock underneath the landslide. The content of B and Sr in DrA is three orders of magnitude greater than the value normally found in shallow springs of NA (a few $\mu g l^{-1}$ as reported by Duchi et al., 2005; Toscani et al., 2001). Considering the data reported in Sect. 2, the long-term interaction between water and host rocks (such as flysch and/or evaporites) cannot in itself justify the measured B values. Mud volcanoes and oilfield waters are consistent with the B contents detected at Ca' Lita, while Sr is much higher than expected. It should be noted that, unlike Sr, B behaves in a more conservative way and hardly precipitates from the solution (Grew and Anovitz, 1996; Walker, 1975).

If mud volcanoes and oil field waters are plotted in a δ^{18}O–Cl graph (Conti et al., 2000), they represent one of the end-members of a hypothetical mixing line connecting

HESSD
9, 7699–7738, 2012

them with shallow GW. GW from Ca' Lita falls on this line (Fig. 7). At the same time, the $\delta^{18}O$–B graph (Fig. 8) makes it possible to separate these two components. Ca' Lita water is completely left-shifted from the mud volcano points, which are polluted by an extra source of B contained in the connate waters of QM. This suggests a purely foredeep origin (oilfield waters) for the Ca' Lita GW.

Leaching experiments on soil samples strengthen this conclusion. In particular, water which interacted with MVRa samples collected at Ca' Lita became more enriched in Na and SO_4 than MVRb leading to the supposition that these clayey outcrops were impregnated with deep water. The interactions with MOH samples (MOHa and MOHb) did not produce any changes in water chemistry and ion contents.

A simple chemical equilibrium analysis was conducted coupling the mineralogical compositions of the soil samples using PHREEQC software. The investigation underlined that, even at equilibrium, the observed levels of Ca and SO_4 cannot be reached. Moreover, there are no local mineralogical phases that could provide Chloride.

7 Discussion: influence of deep water inflow on the groundwater balance of the landslide

The mean annual groundwater recharge from rainfall was estimated using the Thornthwaite and Mather (1957) formula and 40 yr records of rainfall and temperature. A water surplus of 200 mm yr^{-1} was calculated, which is concentrated between December and April (Table 2). A comparison between GW_L variations and the total and effective rainfall calculated for each hydrological year (Thornthwaite and Mather, 1957) is presented in Table 2. A direct relation can easily be observed: the 2006–2007 hydrological year was characterized by the lowest recharge value and consequent minimum GW_L in each piezometer. Conversely, 2009–2010 was very wet and the maximum GW_L was recorded at all points. On the slope scale, the recharge area corresponds to the flysch rock outcropping area, which is about 340 000 m^2. Considering annual water surplus and infiltration area, the mean annual groundwater recharge in the slope can

HESSD
9, 7699–7738, 2012

be estimated in the range of 30 000 to 68 000 m^3, depending on the infiltration coefficients used (0.4 and 1, respectively). Considering aquifer geometry and its storativity coefficient (quantified as 10^{-2} by Ronchetti et al., 2009), the amount of water hosted in the flysch is about 750 000 m^3 (V_f). The annual deep water volume inflow (V_{dw}) at the bottom of the aquifer was estimated by solving a simplified annual water-balance equation and processing the ^3H result according to Mazor (1997). The 3.5 T.U. detected in DrA was due to a mixing of two members, i.e. rain water (10 T.U.) with deep water characterized by long time paths (about O T.U.), aliquots of about 1/3 and 2/3 respectively can be assumed. It should be noted that these proportions are related to the sampling campaign F (August 2010), when the hydrogeological system had already become affected by drainage. Before the drainage network was set-up, the chemical and isotopic analyses suggest a major influence of the deep water component than rain water. Considering the unmodified conditions before the drainage network (pre-2006), the annual input volume V_I (rainfall V_r = 30 000–68 000 m^3 plus deep inflow V_{dw}) in the flysch is assumed equal to the outflow V_{OUT} (Fig. 9). Each component can be linked to the respective oxygen isotope value ($\delta^{18}O_{dw} = +5.5$; $\delta^{18}O_r = -9.13$; $\delta^{18}O_f = -5.33$) and, in this way, the steady-state budget can be expressed as follow:

$$V_r\delta^{18}O_r + V_{dw}\delta^{18}O_{dw} = (V_r + V_{dw})\delta^{18}O_f \quad (1)$$

where:

$$V_{dw} = V_r \cdot \frac{(\delta^{18}O_f - \delta^{18}O_r)}{(\delta^{18}O_{dw} - \delta^{18}O_f)} = 7800\text{–}17\,500\,m^3 \quad (2)$$

depending on the infiltration coefficient used (0.4 and 1, respectively).

The supplemental annual inflow V_{dw} represents about the 26 % of the effective rain which can infiltrate annually through the surface. Although this amount of water is forty times smaller than the volume stored in the deepest aquifer, its constant influx (0.25–0.56 $l\,s^{-1}$) involves a confined unit and it could influence the long term groundwater

HESSD
9, 7699–7738, 2012

level fluctuations. As regards the influence of the additional aliquot of groundwater from deep water inflow on slope stability and on the adequacy of mitigation drainage systems, the following preliminary observations can be made. The groundwater potentiometric surface measured in the hydrologic unit corresponding to the deformation zone exceeds the sliding plane by 35 m. The study demonstrated that this is, at least in part, related to deep water inflow. This implies that draining only the rock slide body, that is the upper hydrologic unit, might not ensure stability in the long term, as deep water inflow could act as a preparatory – if not triggering – factor for further large scale slope instability.

On the other hand, monitoring data from the weirs at the drainage system outlets register around 6000 $m^3 yr^{-1}$ of discharge from DrA, and around 30 000 $m^3 yr^{-1}$ from WA. This value is higher than the estimated deep water annual inflow aliquot, while it is within the range of the estimated total inflow V_I deriving from deep water and rainfall. Therefore, despite the high groundwater potentiometric levels in the deformation zone, these drainage systems are adequately dimensioned to keep the landslide body drained and promote its stability.

8 Conclusion

The paper underlined the utility of coupling hydrology with hydrochemical surveys for quantifying the relative contribution of different sources in slope-scale water budget estimation. A comprehensive hydrogeological study established the inflow of deep water into the hydrological system of Ca' Lita. This inflow originates from an oilfield reservoir hosted at depth, demonstrating that the hydrological boundaries of the system do not correspond with the catchment area of the site. An annual inflow of around 7800–17 500 m^3 of deep water (i.e. 26 % of the annual mean effective rainfall) was assessed. This aliquot represents an additional inflow that cannot be detected by common hydrological investigation and could contribute to the destabilization of the slope. A good understanding of the hydrological limits of a hillslope site is essential when

HESSD
9, 7699–7738, 2012

calculating representative hydrological balances and performing long-term modelling, and this study clearly demonstrates that hydrochemistry should be taken into account whenever the presence of other groundwater sources is suspected.

References

Baraldi, S.: Caratterizzazione idrogeologica, idrochimica e radiometrica di alcuni corpi di frana dell'Appennino Emiliano. Casi di studio: Vedriano, Ca' Lita e Silla, Il Geologo dell'Emilia Romagna, 18, 19–36, 2008.

Bertolini, G. and Gorgoni, C.: La lavina di Roncovetro (Vedriano, Comune di Canossa, Provincia di Reggio Emilia), Quad. Geolog. Appl., 8, 1–21, 2001.

Bettelli, G. and Vannucchi, P.: Structural style of offscraped Ligurian oceanic sequences of the northern Apennines: new hypothesis concerning the development of the melange block-in-matrix fabric, J. Struct. Geol., 25, 371–388, 2003.

Boccaletti, M., Elter, P., and Guazzone, G.: Plate tectonics models for the development of the Western Alps and northern Apennines, Nature, 234, 108–111, 1971.

Bogaard, T., Guglielmi, Y., Marc, V., Emblanch, C., Bertrand, C., and Mudry, J.: Hydrogeochemistry in landslide research: a review, B. Soc. Geol. Fr., 178, 113–126, 2007.

Borgatti, L., Corsini, A., Barbieri, M., Sartini, G., Truffelli, G., Caputo, G., and Puglisi, C.: Large reactivated landslides in weak rock masses: a case study from the Northern Apennines (Italy), Landslides, 3, 115–124, 2006.

Borgatti, L., Corsini, A., Marcato, G., Ronchetti F., and Zabuski, L.: Appraise the structural mitigation of landslide risk via numerical modelling: a case study from the northern Apennines (Italy), Georisk, 2, 141–160, 2008.

Bonini, M.: Interrelations of mud volcanism, fluid venting, and thrust-anticline folding: examples from the external northern Apennines (Emilia-Romagna, Italy), J. Geophys. Res., 112, 1–21, 2007.

Bonzanigo, L., Eberhardt, E., and Loew, S.: Hydromechanical factors controlling the creeping Campo Vallemaggia landslide, in: Proceeding of Landslides-Causes, Impacts and Countermeasures, Davos, Switzerland, 13–22, 2001.

HESSD
9, 7699–7738, 2012

Boschetti, T., Toscani, L., Shouakar-Stash, O., Iacumin, P., Venturelli, G., Mucchino, C., and Frape, S. K.: Salt waters of the northern Apennine Foredeep basin (Italy): origin and evolution, Aquat. Geochem., 17, 71–108, 2010.
Capozzi, R. and Picotti, V.: Fluid migration and origin of a mud volcano in the northern Apennines (Italy): role of deeply rooted normal fault, Terra Nova, 14, 363–370, 2002.
Capozzi, R. and Picotti, V.: Spontaneous fluid emission in the northern Apennines: geochemistry, structures, and implications for the petroleum system, Geol. Soc. Spec. Publ., 348, 115–135, 2010.
Cappa, F., Guglielmi, Y., Soukatchoff, V. M., Mudry, J., Bertrand, C., and Charmoille, A.: Hydromechanical modeling of a large moving rock slope inferred from slope levelling coupled to spring long-term hydrochemical monitoring: example of the La Clapiere landslide (Southern Alps, France), J. Hydrol., 291, 67–90, 2004.
Cervi, F.: Idrologia chimica, isotopica e radiometrica dell'alta Val di Secchia (Chemical, isotopical and radiometrical hydrology of the Upper Secchia Valley), BSc thesis, Università di Modena e Reggio Emilia, Italy, 94 pp., 2003.
Chiesi, M., De Waele, J., and Forti, P.: Origin and evolution of a salty-gypsum/anhydrite karst spring: the case of Poiano (northern Apennines, Italy), Hydrogeol. J., 18, 1111–1124, 2010.
Ciancabilla, N., Borgia, G. C., Bruni, R., Ciancabilla, F., Palmieri, S., and Vicari, L.: Le sorgenti sulfuree dell'alta valle del Reno (Appennino bolognese): nuovi elementi per approfondire la genesi dei movimenti gravitativi profondi nei terreni argillitici caoticizzati dell'Appennino Tosco-Emiliano, Il Geologo dell'Emilia-Romagna, 18, 5–14, 2004.
Colombetti, F. and Nicolodi, F.: La sorgente sulfurea della Frana di Farneta nella valle del Torrente Dolo (Prov. Di Modena) (The sulphurous spring of Farneta's Landslide (Montefiorino, Modena District)), Acta Naturalia de l'Ateneo Parmense, 34, 5–18, 1998.
Conti, A., Sacchi, E., Chiarle, M., Martinelli, G., and Zuppi, G. M.: Geochemistry of the formation waters in the Po plain (northern Italy), Appl. Geochem., 15, 51–65, 2000.
Corsini, A., Borgatti, L., Cervi, F., Dahne, A., Ronchetti, F., and Sterzai, P.: Estimating mass-wasting processes in active earth slides – earth flows with time-series of High-Resolution DEMs from photogrammetry and airborne LiDAR, Nat. Hazards Earth Syst. Sci., 9, 433–439, doi:10.5194/nhess-9-433-2009, 2009.
Cremaschi, F.: Evidenze isotopiche, chimico-fisiche e piezometriche della circolazione idrica sotterranea in acquiferi fratturati e porosi dell'Appennino settentrionale (Monte Modino, Alta Val Secchia) (Isotopical, chemical and piezometric evidences of groundwater circulation

HESSD
9, 7699–7738, 2012

through fractured and porous aquifers of the northern Apennines), BSc Thesis, Università di Modena e Reggio Emilia, Italy, 115 pp., 2008.
Cruden, D. M. and Varnes, D. J.: Landslides types and processes, in: Landslides: Investigation and Mitigation, Special Report, edited by: Turner, A. K. and Schuster, R. L., Transportation Research Board, National Academy Press, Washington DC, 247, 36–75, 1996.
de Montety, V., Marc, V., Emblanch, C., Malet, J. P., Bertrand, C., Maquaire, O., and Bogaard, T. A.: Identifying the origin of groundwater and flow processes in complex landslides affecting black marls: insights from a hydrochemical survey, Earth Surf. Process. Landforms, 32, 32–48, 2007.
Drever, J. I.: The Geochemistry of Natural Waters: Surface and Groundwater Environments, 3rd edn., Prentice Hall, Upper Saddle River, 1997.
Duchi, V., Venturelli, G., Boccasavia, I., Bonicolini, F., Ferrari, C., and Poli, D.: Studio geochimico dei fluidi dell'Appennino Tosco-Emiliano-Romagnolo, Boll. Soc. Geol. It., 124, 475–491, 2005.
Fazlagic, S., Lombroso, L., and Quattrocchi, S.: Osservazioni meteorologiche 2004 a Modena e Ferrara, Atti Società Naturalisti e Matematici di Modena, 135, 5–40, 2004.
Freeze, R. A. and Cherry, J. A.: Groundwater, Prentice-Hall, Englewood Cliffs, NJ, 604 pp., 1979.
Gargini, A., Vincenti, V., Piccinini, L., Zuppi, G. M., and Canuti, P.: Groundwater flow systems in turbidites of the northern Apennines (Italy): natural discharge and high speed railway tunnel drainage, Hydrogeol. J., 16, 1577–1599, 2008.
Gran, G.: Determination of the equivalence point in in the potentiometric titrations, Analyst, 77, 661–671, 1952.
Grew, E. S. and Anovitz, L. M.: Boron: mineralogy, petrology and geochemistry, Rev. Mineral., 33, 864 pp., 1996.
Guglielmi, Y., Bertrand, C., Compagnon, F., Follacci, J. P., and Mudry, J.: Acquisition of water chemistry in a mobile fissured basement massif: its role in the hydrogeological knowledge of the La Clapiere landslide (Mercantour massif, Southern Alps, France), J. Hydrol., 229, 138–148, 2000.
Heinicke, J., Italiano, F., Koch, U., Martinelli, G., and Tedesca, L.: Anomalous fluid emission of a deep borehole in a seismically active area of northern Apennines (Italy), Appl. Geochem., 25, 555–571, 2010.

HESSD
9, 7699–7738, 2012

Hutchinson, J. N.: A coastal mudflow on the London Clay cliffs at Beltinge, North Kent, Geotechnique, 20, 412–438, 1970.
Iacumin, P., Venturelli, G., and Selmo, E.: Isotopic features of rivers and groundwater of the Parma Province (northern Italy) and their relationships with precipitation, J. Geochem. Explor., 102, 56–62, 2009.
Iverson, R. M. and Major, J. J.: Rainfall, groundwater flow, and seasonal motion at Minor Creek landslide, Northwestern California: physical interpretation of empirical relations, Geol. Soc. Am. Bull., 99, 579–594, 1987.
Kligfield, R.: The northern Apennines as a collisional orogen, Am. J. Sci., 279, 676–691, 1979.
Longinelli, A. and Selmo, E.: Isotopic composition of precipitation in Italy: a first overall map, J. Hydrol., 270, 75–88, 2003.
Martinelli, G. and Dadomo, A.: Geochemical model of mud volcanoes from reviewed worldwide data, short review, in: Mud Volcanoes, Geodynamics and Seismicity, NATO Sciences Series IV: Earth and Environmental Sciences, 51, 211–220, 2005.
Martinelli, G. and Judd, A.: Mud volcanoes of Italy, Geol. J., 39, 49–61, 2004.
Martinelli, G., Bassignani, A., Ferrari, G., and Finazzi, P. B.: Predicting earthquakes in northern Apennines: recent developments in monitoring Radon-222, in: Proceedings of the 4th Int. Symp. on the Analysis of Seismicity and Seismic Risk, 192–208, Bechyne Castel, Czechoslovakia, 2–8 September, 1989.
Mazor, E.: Chemical and Isotopic Groundwater Hydrology, Marcel Dekker Inc., New York, 413 pp., 1997.
Minissale, A., Magro, G., Martinelli, G., Vaselli, O., and Tassi, F.: Fluid geochemical transect in the northern Apennines (Central-Northern Italy): fluid genesis and migration and tectonic implications, Tectonophysics, 319, 199–222, 2000.
Molli, G.: Northern Apennine-Corsica orogenic system: an update overview, Geol. Soc. Spec. Publ., 298, 413–442, 2008
Papani, G., De Nardo, M. T., Bettelli, G., Rio, D., Tellini, C., and Vernia, L.: Note Illustrative della Carta Geologica d'Italia alla scala 1 : 50.000, Foglio 218 Castelnovo Ne' Monti, Servizio Geologico d'Italia, Roma, 139 pp., 2002.
Parkhurst, D. L. and Appelo, C. A. J.: PHREEQC2 user's manual and program, Water-Resources Investigations Report, edited by: US Geological Survey, Denver, Colorado, 2004.
Regione Emilia-Romagna – ARPA: Caratterizzazione geochimica dell'acquifero superficiale e definizione del suo stato di contaminazione, in: Progetto di Fattibilità per la Bonifica

HESSD
9, 7699–7738, 2012

dell'Acquifero Superficiale dell'Area del Distretto Ceramico di Modena e Reggio Emilia, Bologna, 122 pp., 2009.
Ronchetti, F., Borgatti, L., Cervi, F., Gorgoni, C., Piccinini, L., Vincenzi, V., and Corsini, A.: Groundwater processes in a complex landslide, northern Apennines, Italy, Nat. Hazards Earth Syst. Sci., 9, 895–904, doi:10.5194/nhess-9-895-2009, 2009.
Thatcher, L. L., Janzer, V. J., and Edwards, R. W.: Methods for determination radioactive substances in water and fluvial sediments, in: Techniques of Water Resources Investigations, edited by: US Geological Survey, Washington, 79–81, 1977.
Thornthwaite, C. W. and Mather, J. R.: Instruction and tables for computing potential evapotraspiration and the water balance, Publ. Clim. Drexel Inst. Technol., 10, 185–311, 1957.
Tóth, J.: Groundwater as a geological agent: an overview of the causes, processes, and manifestation, Hydrogeol. J., 7, 1–14, 1999.
Tóth, J.: Gravitational Systems of Groundwater Flow: Theory, Evaluation, Utilization, Cambridge University Press, Cambridge, 297 pp., 2009.
Toscani, L., Venturelli, G., and Boschetti, T.: Sulphide-bearing waters in northern Apennines, Italy: general features and water–rock interaction, Aquat. Geochem., 7, 195–216, 2001.
USGS: A simple field leach test to assess potential leaching of soluble constituents from mine wastes, soils, and other geologic materials, USGS Fact Sheet, Denver, Colorado, 2005–3100, 2005.
van Asch, T. W. J., Buma, J., and Van Beek, L. P. H.: A view on some hydrological triggering systems in landslides, Geomorphology, 30, 25–32, 1999.
Vannucchi, P., Remitti, F., and Bettelli, G.: Geological record of fluid flow and seismogenesis along an erosive subducting plate boundary, Nature, 451, 699–703, 2008.
Venturelli, G., Boschetti, T., and Duchi, V.: Na-carbonate waters of extreme composition: possible origin and evolution, Geochem. J., 37, 351–366, 2003.
Walker, C. T.: Geochemistry of Boron, Dowden, Hutchinson & Ross, Benchmark Papers in Geology, Stroudsburg, PA, 23, 414 pp., 1975.
White, D. E.: Saline waters of sedimentary rocks, Am. Assoc. Petr. Geol. Mem., 4, 342–366, 1965.
Wieczorek, G. F.: Landslide triggering mechanisms, in: Landslides Investigation and Mitigation, edited by: Turner, A. K. and Schuster, R. L., special report, 247, National Academy Press, Washington DC, 1996.

HESSD
9, 7699–7738, 2012

WP/WLI: Working Party on the World Landslide Inventory and Canadian Geotechnical Society, Multilingual Landslide Glossary, edited by: Richmond, B. C., BiTech Publishers, British Columbia, Canada, 59 pp., 1993.

HESSD
9, 7699–7738, 2012

Table 1. Characteristics of piezometers, wells and drainage systems in the Ca' Lita landslide. Depth of the main slip and filters are also reported.

Name	Location	Slotted from–to (m)	Altitude (m a.s.l.)	Depth of the main sliding surface (m)	Continuous level/discharge monitoring	Continuous conductivity-monitoring
P1	Rock slide	9–50	631	6	X	
P2	Rock slide	4–59	539	17–35	X	
P3	Rock slide body	3–44	520	44	X	X
P4	Below the main slide surface	50–59	520	44	X	X
P5	Below the main slide surface	55–60	525	48	X	
WA	Below the main slide surface	50–59	521	44	X	
DrA	Below the main slide surface	about 55	465	44	X	
DrB	Superficial debris	about 13	455	13		

HESSD
9, 7699–7738, 2012

Table 2. Piezometer monitoring and total-effective rainfall. Data are distinguished by hydrologic year.

Pz	Hydrologic year	GW_L max (m a.s.l.)	GW_L min (m a.s.l.)	GW_Lmax-GW_Lmin (m)	Mean GW_L	Mean air temp (°C)	Mean rainfall (mm)	Mean effective rainfall (mm)
P1	2005–2006	623.62	616.16	8.71	618.39	12.3	880	273
P2		523.35	520.70	2.65	522.22			
P3		–	–	–	491.76			
P4		513.77	508.98	4.79	510.16			
P5		–	508.47	–	–			
P1	2006–2007	621.19	614.33	6.86	616.03	14.5	763	49
P2		520.7	518.42	2.28	519.46			
P3		–	–	–	490.19			
P4		509.75	508.33	1.42	508.5			
P5		510.79	509.72	1.07	510.4			
P1	2007–2008	623.33	616.24	7.09	618.14	12.7	845	299
P2		519.19	517.99	1.2	518.41			
P3		–	–	–	488.73			
P4		513.65	502.43	11.22	508.96			
P5		512.21	507.89	4.32	510.97			
P1	2008–2009	624.47	616.18	8.29	619.37	12.7	893	447
P2		526.93	–	–	–			
P3		–	–	–	488.5			
P4		518.10	508.21	9.89	512.33			
P5		513.56	511.60	2.15	512.27			
P1	2009–2010	624.90	–	–	–	12.5	1152	347
P2		–	–	–	–			
P3		–	–	–	488.50			
P4		518.26	–	–	–			
P5		514.17	–	–	–			

HESSD
9, 7699–7738, 2012

Table 3. Groundwater chemical (sampling campaign A, B, D) and isotopic (sampling campaign B, C, D, E, F) analyses of the Ca' Lita samples. Other samples are reported for further comparison: mud volcanoes (point: 3b), common shallow groundwater (point: 5) and hydrocarbon seep (point: 8).

Group	Sampling campaign	Name	pH	T (°C)	Electrical Conduct. −25 °C ($\mu S\,cm^{-1}$)	pCO_2 (kPa)	Ca ($mg\,l^{-1}$)	Mg ($mg\,l^{-1}$)	Na ($mg\,l^{-1}$)	K ($mg\,l^{-1}$)	Sr ($mg\,l^{-1}$)	B ($mg\,l^{-1}$)	HCO_3 ($mg\,l^{-1}$)	Cl ($mg\,l^{-1}$)	SO_4 ($mg\,l^{-1}$)	δ^2H	$\delta^{18}O$
1	A	DrB	n.a.	n.a.	2641	2.0	67.1	47.3	464	9.0	n.a.	n.a.	195	53	1110	n.a.	n.a.
1	A	P1	6.6	15.0	4015	2.6	13.2	16.0	885	3.0	n.a.	n.a.	292	425	1140	n.a.	n.a.
1	A	P3	7.4	16.0	2767	1.6	5.5	1.6	619	9.9	n.a.	n.a.	171	71	1095	n.a.	n.a.
1	A	P5	7.5	15.0	2243	1.8	23.1	13.2	462	2.4	n.a.	n.a.	195	88	795	n.a.	n.a.
1	B	DrA	7.6	n.a.	5088	4.7	7.9	6.2	1155	3.0	n.a.	n.a.	525	787	980	−49.23	−5.33
1	B	P1	n.a.	n.a.	n.a.	n.a.	n.a.	n.a.	n.a.	n.a.	n.a.	n.a.	n.a.	n.a.	n.a.	−52.47	−6.51
1	B	P2	7.1	16.0	3818	3.0	13.8	8.8	858	3.2	n.a.	n.a.	348	313	1160	n.a.	n.a.
1	B	P3	n.a.	n.a.	n.a.	n.a.	n.a.	n.a.	n.a.	n.a.	n.a.	n.a.	n.a.	n.a.	n.a.	−59.03	−8.05
1	B	P4	7.0	15.0	4362	9.1	14.3	7.9	1045	4.2	n.a.	n.a.	1050	35	1400	n.a.	n.a.
1	B	P5	n.a.	n.a.	n.a.	n.a.	n.a.	n.a.	n.a.	n.a.	n.a.	n.a.	n.a.	n.a.	n.a.	−63.77	−9.13
1	C	DrA	n.a.	n.a.	n.a.	n.a.	n.a.	n.a.	n.a.	n.a.	n.a.	n.a.	n.a.	n.a.	n.a.	−47.99	−5.33
1	C	P3	n.a.	12.8	3300	n.a.	n.a.	n.a.	n.a.	n.a.	n.a.	n.a.	n.a.	n.a.	n.a.	−56.28	−7.73
1	C	P4	n.a.	12.5	4390	n.a.	n.a.	n.a.	n.a.	n.a.	n.a.	n.a.	n.a.	n.a.	n.a.	−60.56	−8.51
1	C	P5	n.a.	11.7	3770	n.a.	n.a.	n.a.	n.a.	n.a.	n.a.	n.a.	n.a.	n.a.	n.a.	−63.88	−9.13
1	D	DrA	7.4	n.a.	7577	4.1	146.0	67.0	1660	22.0	6.8	8.2	529	416	3130	−52.38	−6.80
1	D	P1	7.1	18.0	4575	9.1	98.0	37.0	970	14.0	3.4	6.4	1129	189	1280	−54.98	−7.90
1	D	P2	6.9	14.3	n.a.	n.a.	n.a.	n.a.	n.a.	n.a.	n.a.	n.a.	n.a.	n.a.	n.a.	−58.66	−8.58
1	D	P4	n.a.	15.0	n.a.	n.a.	n.a.	n.a.	n.a.	n.a.	n.a.	n.a.	n.a.	n.a.	n.a.	−57.78	−8.73
1	D	P5	7.6	15.0	2330	n.a.	n.a.	n.a.	n.a.	n.a.	n.a.	n.a.	n.a.	n.a.	n.a.	−61.35	−9.22
1	E	P2	n.a.	n.a.	n.a.	n.a.	n.a.	n.a.	n.a.	n.a.	n.a.	n.a.	n.a.	n.a.	n.a.	−66.00	−9.88
1	E	P4	7.1	13.1	5730	n.a.	n.a.	n.a.	n.a.	n.a.	n.a.	n.a.	n.a.	n.a.	n.a.	−58.53	−8.60
1	F	DrA	7.3	n.a.	9540	n.a.	n.a.	n.a.	n.a.	n.a.	n.a.	n.a.	n.a.	n.a.	n.a.	−53.54	−6.93
5	D	Pavullo	n.a.	n.a.	n.a.	n.a.	n.a.	n.a.	n.a.	n.a.	n.a.	n.a.	n.a.	n.a.	n.a.	−62.28	−9.65
5	D	Serra-mazzoni	n.a.	n.a.	n.a.	n.a.	n.a.	n.a.	n.a.	n.a.	n.a.	n.a.	n.a.	n.a.	n.a.	−63.64	−9.90
5	D	Lusino	7.1	16.0	681	n.a.	n.a.	n.a.	n.a.	n.a.	n.a.	n.a.	n.a.	n.a.	n.a.	−60.78	−9.33
5	D	Nismozza	7.8	n.a.	274	1.5	41.0	6.0	13	1.1	0.6	0.0	152	5	31	n.a.	−9.17
8	D	Rio Petrolio	8.1	n.a.	6619	13.6	13.0	20.0	1445	27.0	1.5	11.9	1534	1480	4	n.a.	−7.71
3b	D	Monte Gibbio	7.6	n.a.	33 739	0.7	163.0	160.0	7500	63.0	28.7	66.5	584	12 690	2	n.a.	5.00

HESSD
9, 7699–7738, 2012

Table 4. Leaching results for the 4 soil samples collected. Chemical analyses for the 1h samples are also reported in mgl^{-1}.

	Electrical conductivity –25 °C ($\mu S\,cm^{-1}$)								
Soil sample	30 s	1 m	2 m	5 m	10 m	30 m	1 h	5 h	10 h
MOHa	68	106	133	157	193	196	206	222	228
MVRa	460	615	694	817	924	855	861	754	928
MOHb	78	107	135	192	198	205	244	249	251
MVRb	81	96	112	123	140	148	179	194	199

	Chemical data						
Soil sample	Na	Mg	Ca	K	SO_4	Cl	HCO_3
MOHa	40	2	5	1	12	0	113
MVRa	160	4	8	3	175	5	210
MOHb	25	3	20	2	16	0	120
MVRb	10	2	18	1	10	0	107

HESSD
9, 7699–7738, 2012

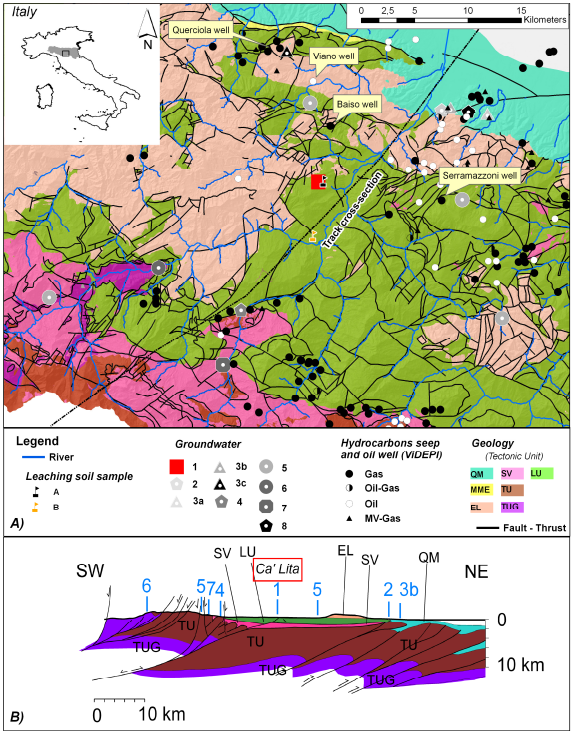

Fig. 1. (a) Simplified map of geologic units of the northern Apennines. **(b)** Geological cross-section (modified after Vannucchi et al., 2008). Legend: geologic units (TU: Tuscan Units; TUG: Triassic Evaporites; LU: Ligurian units; EL: Epiligurian Units; SV: Sestola-Vidiciatico unit; MME: Messinian Evaporites; QM: Post Messinian Units). Water springs, water samples, hydrocarbon seeps and oil wells (1: Ca' Lita samples; 2: Salvarola baths; 3a: Mud volcano Nirano; 3b: Mud volcano Monte Gibbio; 3c: Mud volcano Regnano; 4: Quara baths; 5: Common shallow groundwater; 6: Poiano spring; 7: Morsiano spring; 8: Rio Petrolio hydrocarbon seep) Soil samples for leaching experiments (A: weathered Ca' Lita material; B: in situ rock outcrop).

HESSD
9, 7699–7738, 2012

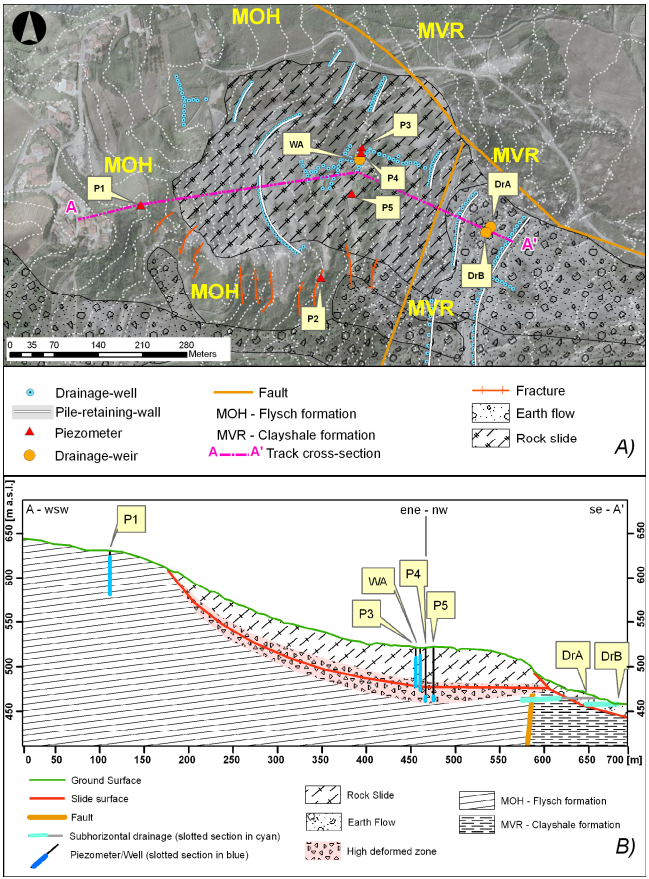

Fig. 2. (a) Geological sketch of Ca' Lita landslide. Location of the monitoring points: DrA, DrB and piezometers. **(b)** Geological cross-section of Ca' Lita with drainage and monitoring works.

HESSD
9, 7699–7738, 2012

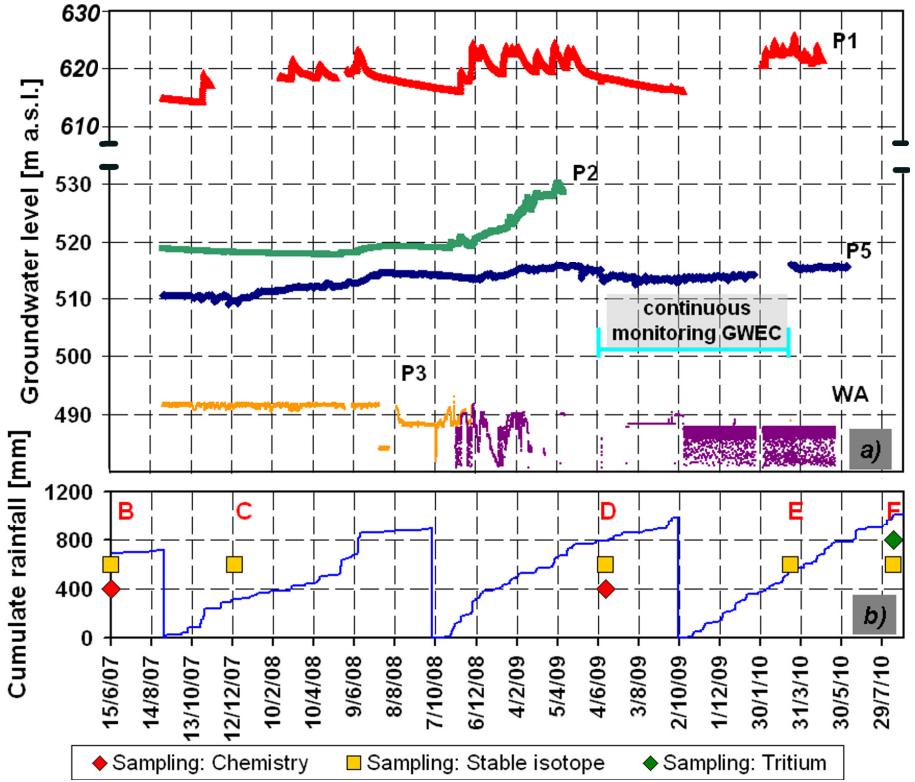

Fig. 3. (a) Continuous GW_L monitoring for piezometers P1, P2, P3, P5. **(b)** Cumulative rainfall for each hydrologic year. Chemical (red square) and isotopic (yellow diamond: stable isotopes; green diamond: tritium) sampling campaigns are reported.

HESSD
9, 7699–7738, 2012

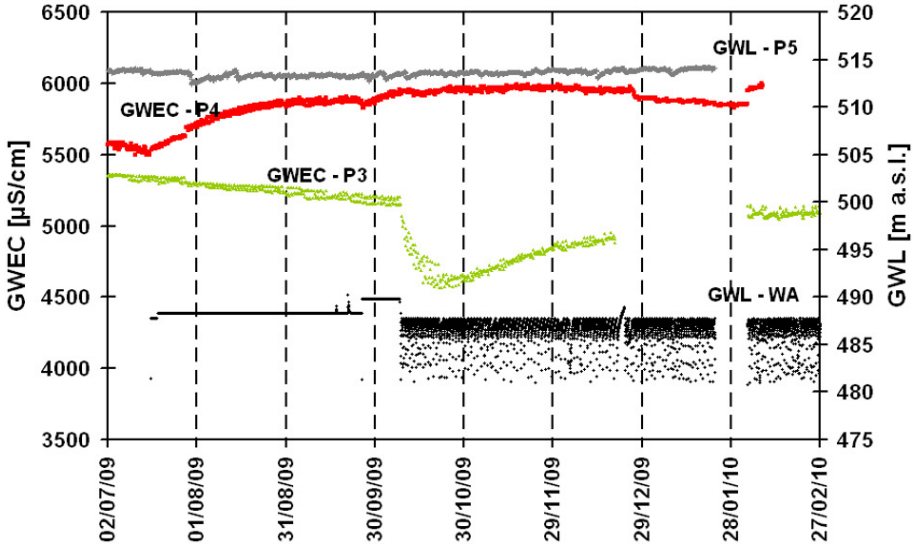

Fig. 4. Continuous GW_{EC} monitoring for piezometers P3 and P4 and GW_L in WA and P5.

HESSD
9, 7699–7738, 2012

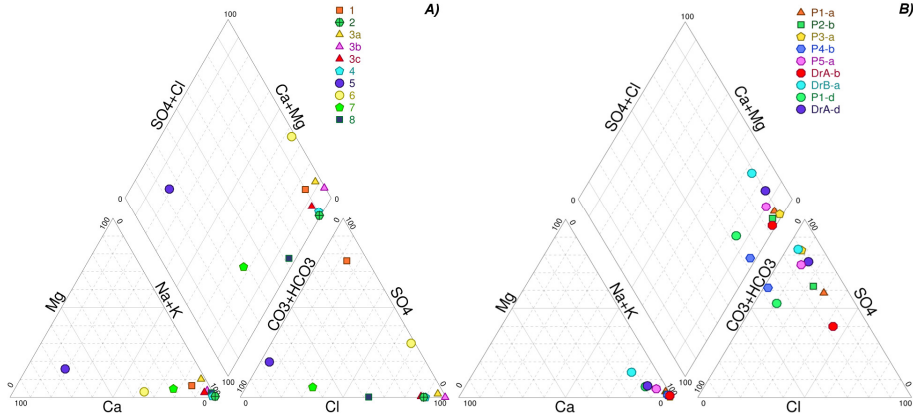

Fig. 5. Piper diagram. **(a)** Water sample DrA compared with common shallow groundwater (point: 5), other springs (point: 6 – Cervi, 2003; 7 – Venturelli et al., 2003), mud volcanoes (point: 3a, c – Martinelli et al., 1989), baths (point: 2, 4 – Boschetti et al., 2010), and hydrocarbon seep (point: 8) as described in Fig. 1a. **(b)** Ca' Lita water samples from the B and D campaigns.

HESSD
9, 7699–7738, 2012

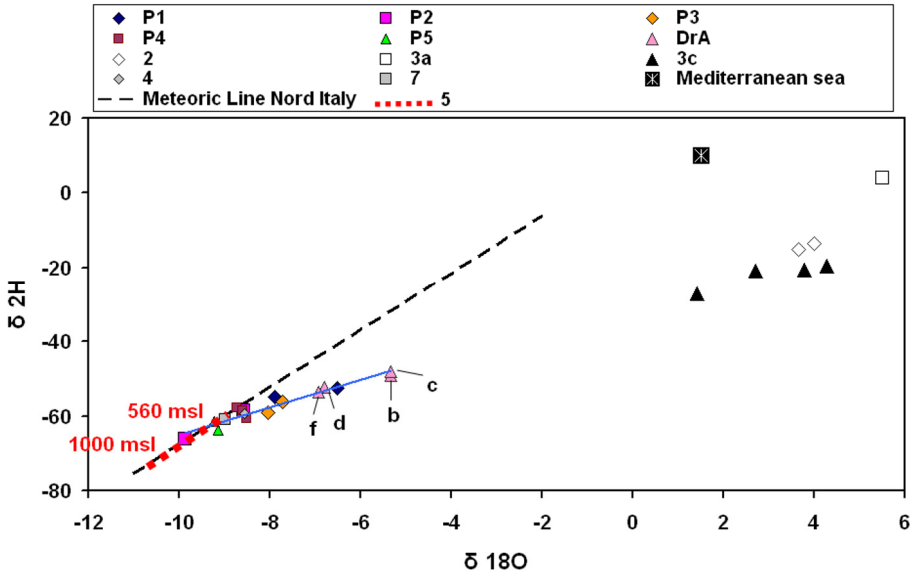

Fig. 6. $\delta^{18}O$–$\delta^{2}H$ diagram. DrA point sampling campaigns are reported. Point: 2, 4 (Boschetti et al., 2010) – baths; 3a (Conti et al., 2000), 3c (Capozzi and Picotti, 2010) – mud volcanoes; 7 (Venturelli et al., 2003) – spring. Red dashed line was obtained from 5-common shallow groundwater. Blue line represents the alignment of the $\delta^{2}H$ depleted samples at Ca' Lita. Black dashed line is the mean isotopic relation for rainfalls in northern Italy (Longinelli and Selmo, 2003).

HESSD
9, 7699–7738, 2012

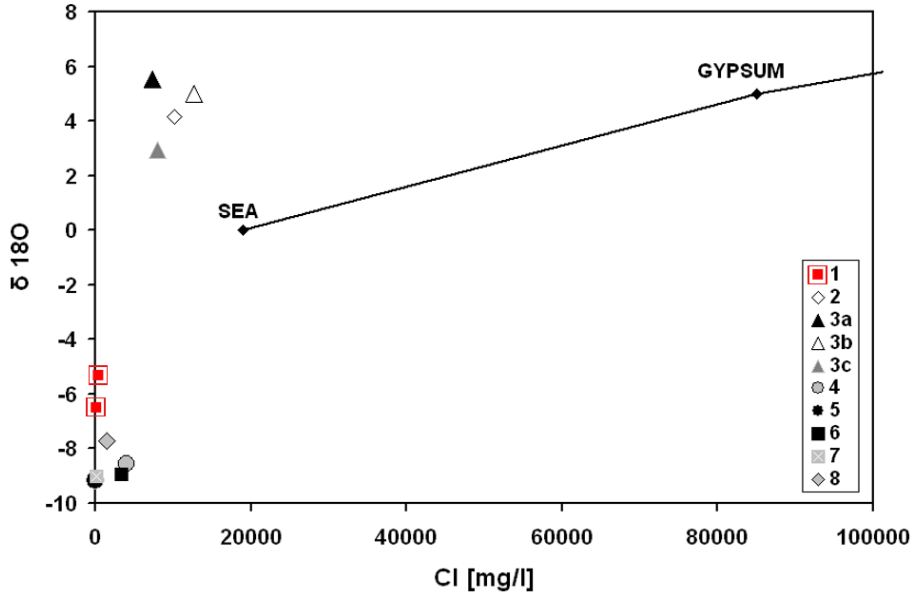

Fig. 7. δ^{18}O–Cl diagram. Point: 2, 4 (Boschetti et al., 2010) – baths; 3a (Conti et al., 2000), 3b,c (Capozzi and Picotti, 2010) – mud volcanoes; 5-common shallow groundwater; 6 (Cervi, 2003), 7 (Venturelli et al., 2003) – spring; 8-hydrocarbon seep. Black line: evaporation line from seawater.

HESSD
9, 7699–7738, 2012

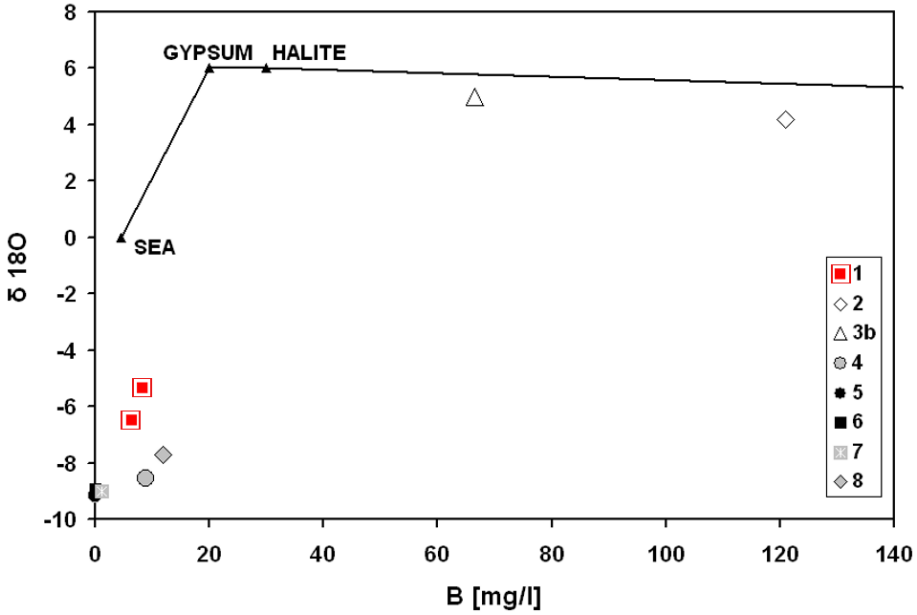

Fig. 8. δ^{18}O–B diagram. Point: 2, 4 (Boschetti et al., 2010) – baths; 3b – mud volcanoes; 5-common shallow groundwater; 6 (Cervi, 2003), 7 (Venturelli et al., 2003) – spring; 8-hydrocarbon seep. Black line: evaporation line from seawater.

HESSD
9, 7699–7738, 2012

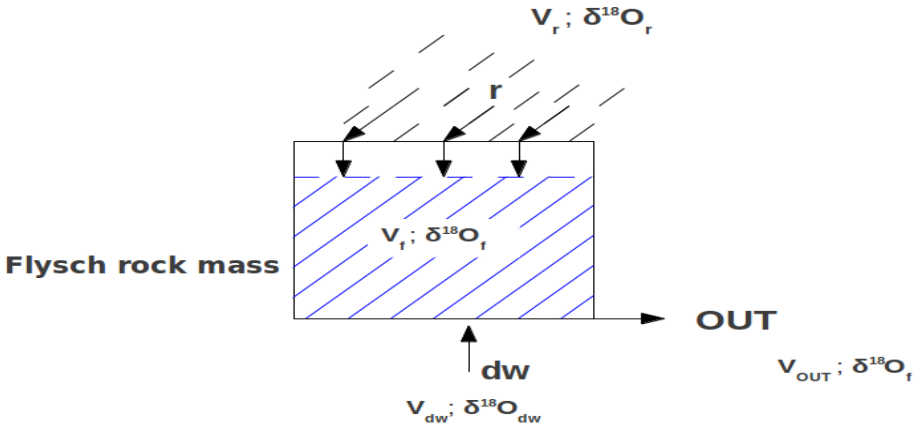

Fig. 9. Reservoir-concept model of the slope. Water volumes (V_r: annual rainfall volume; V_{dw}: annual deep water volume inflow; V_f: mean annual volume of water hosted inside the flysch; V_{OUT}: annual water outflow volume) and their corresponding isotopic signals.

HESSD
9, 7699–7738, 2012